Check for updates

ADVANCED ENGINEERING MATERIALS
www.aem-journal.com

Encapsulating Laser-Induced Graphene to Preserve its Electrical Properties and Enhance its Mechanical Robustness

*Fatemeh Bayat, Mohammad Nazeri, Gerd Grau, and Simone Pisana**

Laser-induced graphene (LIG) has gained significant attention as a promising material for various applications, including flexible electronics, due to its high electrical conductivity, ease of fabrication, and cost-effective production. However, its fragile structure makes it susceptible to degradation under mechanical stress and harsh environments. Existing encapsulation techniques compromise LIG's conductivity, limiting its practical applications. Herein, an encapsulation method that enhances the mechanical durability while preserving its electrical properties is introduced. The LIG exhibits an initial sheet resistance of 2.2 $\Omega\,sq^{-1}$, which is among the lowest values ever achieved. Using a pressure of 80 psi, LIG is encapsulated with a polyimide layer, resulting in a minimal resistance increase of only 5%. Comprehensive characterization, including Raman spectroscopy and scanning electron microscopy, confirms that the encapsulation approach maintains the structural integrity of LIG while significantly improving its resilience to bending and environmental factors such as moisture and temperature fluctuations. Additionally, initial cyclic loading tests demonstrate the encapsulated LIG's ability to retain most of its conductive properties after the first mechanical deformation. These findings highlight the potential of this encapsulation technique for advancing flexible and wearable electronic devices, paving the way for more durable, high-conductivity graphene-based technologies.

1. Introduction

Graphene, a 2D monolayer of carbon atoms arranged in a hexagonal honeycomb structure, has gained widespread attention due to its exceptional electrical, mechanical, and thermal properties. Serving as the fundamental building block for various carbon allotropes, including fullerenes, carbon nanotubes, and graphite, graphene has been extensively studied since its isolation in 2004 by Geim and Novoselov, leading to advancements across fields such as electronics, energy storage, and biomedical applications.[1–5] Its unique properties, including high surface area,[6–8] ultra-high carrier mobility,[9] high thermal conductivity,[10,11] ultra-thin thickness,[12] and chemical stability,[13] have positioned it as a revolutionary material in nanotechnology.

Among the numerous methods for graphene fabrication,[14] laser-induced graphene (LIG) has emerged as a promising technique due to its simplicity, cost-effectiveness, and scalability. Unlike conventional methods such as hydrothermal,[7,15] chemical reduction,[16,17] chemical vapor deposition (CVD),[18,19] and template-directed synthesis,[20,21] which often require high temperatures, hazardous chemicals, and multistep processes, LIG offers a rapid, one-step approach for converting carbon-rich polymers into porous graphene structures using laser irradiation. Initially demonstrated in 2014, this process enables direct graphene patterning on polyimide (Kapton) substrates using a CO_2 laser without vacuum conditions, chemical treatments, or transfer steps, making it highly attractive for industrial applications.[22,23] The process involves ultrafast photothermal conversion, wherein high-intensity laser pulses induce rapid heating ($\approx 10^5$ °C s^{-1}), breaking chemical bonds and restructuring carbon into a graphene-like network. This transformation primarily converts sp^3-hybridized carbon into sp^2-hybridized graphene while preventing complete oxidation through localized oxygen depletion and rapid gas release (CO and CO_2).[23–29]

LIG exhibits a porous, 3D interconnected structure with high electrical conductivity, mechanical flexibility, and surface area, making it ideal for energy storage devices (supercapacitors, batteries),[6,22,30–32] wearable electronics,[25,33] and electrochemical sensors.[6,34–37] Additionally, it has been explored for sustainable applications such as water treatment and fuel cell electrodes.[6,30] The electrical conductivity of LIG ($\approx$25 S cm^{-1}) is comparable to graphite perpendicular to its basal plane (3–25 S cm^{-1}) and higher than most semiconductors (10^{-8}–10^{2} S cm^{-1}) but remains two or more orders of magnitude lower than metals ($>10^4$ S cm^{-1}).[38,39] However, despite its promising attributes, LIG's practical implementation is hindered by its inherent mechanical fragility.[40,41]

One of the key limitations of LIG is its susceptibility to cracking and degradation under even mild mechanical stress, which poses challenges for applications requiring repeated deformation.[36,42] While its porous structure enhances conductivity, it also weakens

F. Bayat, M. Nazeri, G. Grau, S. Pisana
Department of Electrical Engineering and Computer Science
York University
4700 Keele Street, Toronto, ON M3J 1P3, Canada
E-mail: pisana@yorku.ca

The ORCID identification number(s) for the author(s) of this article can be found under https://doi.org/10.1002/adem.202501686.

© 2025 The Author(s). Advanced Engineering Materials published by Wiley-VCH GmbH. This is an open access article under the terms of the Creative Commons Attribution-NonCommercial-NoDerivs License, which permits use and distribution in any medium, provided the original work is properly cited, the use is non-commercial and no modifications or adaptations are made.

DOI: 10.1002/adem.202501686

15272648, 0, Downloaded from https://advanced.onlinelibrary.wiley.com/doi/10.1002/adem.202501686, Wiley Online Library on [24/09/2025]. See the Terms and Conditions (https://onlinelibrary.wiley.com/terms-and-conditions) on Wiley Online Library for rules of use; OA articles are governed by the applicable Creative Commons License

mechanical integrity. Additionally, substrate adhesion varies based on laser processing conditions, and mechanical stresses such as bending, stretching, and surface abrasion can introduce microcracks and increased resistance over time.[43–45] Furthermore, humidity and temperature fluctuations can accelerate oxidation and degrade electrical performance,[46,47] emphasizing the need for stabilization strategies to improve mechanical durability and environmental stability.

To address these challenges, researchers have explored encapsulation techniques to enhance LIG's mechanical robustness while maintaining high conductivity. Protective polymer coatings, such as polydimethylsiloxane (PDMS)[45,48,49] and parylene, shield the LIG surface from environmental factors, but significantly increase sheet resistance (e.g., from 0.13 to 0.97 kΩ sq^{-1} with polyurethane encapsulation, and from 1.5 to 15.9 kΩ sq^{-1} using thermal evaporation SiO_2).[45,48] In Spasenović et al., adhesive tape was manually pressed onto the LIG surface and peeled off to assess damage, with the change in resistance reported as a percentage. For LIG on commercial PI, the resistance increased by more than 400%, from ≈400 Ω to 2 kΩ, indicating extremely weak adhesion. A similar trend was observed for LIG on PU-30st,-40st,-50st (wt% soft segment content), where the resistance increased by ≈375% (from 2.1 to 10 kΩ), ≈110%, from 2.1 to 4.4 kΩ, and less than 30% (from 6.6 to 8.5 kΩ) respectively.[50] Similarly, embedding LIG into epoxy resins or thermoplastic polymers enhances durability but often compromises electrical performance.[24,40,43,45] Plasma treatment techniques, such as cold Argon plasma, have been shown to increase graphene crystallinity by 21% and improve electrical conductivity by 51.13%, which can enhance the structural integrity and electrical stability of LIG under operational stress. Additionally, gold nanoparticle coatings enhance triboelectric properties, potentially contributing to better durability in energy-harvesting applications, though their effect on conductivity remains underexplored.[51,52] Another approach involves laser processing parameter optimization, where modifying laser power and scan speed produces denser graphene networks with improved resilience, yet does not fully address LIG's mechanical fragility under stress.[53]

This study aims to develop a novel and simple encapsulation method to improve LIG's mechanical durability while preserving its high electrical conductivity. We introduce a hydraulic press encapsulation technique, where an additional polyimide layer is applied under controlled pressure. This approach maintains LIG's electrical properties while significantly enhancing its resistance to mechanical stress and environmental degradation. To systematically assess this method, we optimize applied pressure to minimize its impact on electrical resistance while improving structural integrity. The encapsulated LIG samples undergo electrical, structural, and mechanical characterization using Raman spectroscopy, scanning electron microscopy (SEM) imaging, cyclic loading tests, and environmental durability studies. These investigations will evaluate our method's effectiveness in preserving LIG's conductivity, flexibility, and environmental stability. By enhancing the mechanical resilience of LIG while maintaining its electrical performance, this study provides a foundation for future research and real-world applications requiring both high conductivity and structural integrity.

2. Experimental Section

2.1. Fabrication of LIG

The fabrication of LIG was performed using a 10.6 μm wavelength CO_2 laser cutter (Hydra 16A) from Hyrel 3D (Atlanta, GA), which selectively patterned graphene structures onto Kapton (polyimide) substrates with silicone adhesive (CGSTAPE-8458, Creative Global Services (CGS), Newmarket, ON). The primary substrate used was a flexible adhesive polyimide sheet with a total thickness of 250 μm. The substrate was prepared by stacking two layers of Kapton tape (each 127 μm thick, excluding adhesive), with the adhesive sides pressed together to form a single ≈250 μm-thick structure. The laser patterning process was conducted under ambient conditions, eliminating the need for vacuum environments or additional processing chemicals. The laser was programmed to inscribe rectangular patterns, measuring 36 mm × 2 mm, using vector mode for lengthwise features and raster mode for widthwise features. The laser's focal distance was 8 mm and the beam spot size was ≈400 μm.

The laser parameters were optimized to achieve LIG with low sheet resistance. In our case, this was obtained at a laser power of 45% of the 40 W maximum (18 W) to ensure controlled photothermal decomposition without excessive ablation. Additionally, a pulse spacing of 1000 dots per inch and a scan rate of 700 mm per minute were selected, with a temporal spacing between laser pulses of 2.178 ms. **Figure 1** illustrates the laser scribing process, the resulting LIG microstructure, and the hydraulic press encapsulation method, providing a graphical representation of the CO_2 laser beam interacting with the Kapton substrate and how LIG fabricated on the Kapton substrate is encapsulated with an additional polyimide layer under controlled pressure. The inset displays a SEM image of the porous LIG surface.

The optimal laser settings were selected through a systematic variation of power and scan rate. The laser power was adjusted between 15% (6 W) and 80% (32 W), while the scan rate was varied from 200 mm per minute to 1500 mm per minute.

2.2. LIG Encapsulation

Given the inherent mechanical fragility of LIG, encapsulation was necessary to improve its durability while preserving its electrical properties. The encapsulation technique described here is scalable and is implemented using a hydraulic press to sandwich LIG between two polyimide layers under controlled pressure. This process was optimized to enhance resistance to mechanical stress and environmental degradation while maintaining the original material conductivity.

Since the LIG was fabricated on a Kapton substrate to begin with, the encapsulation process involved placing an additional 125 μm-thick adhesive-backed Kapton sheet over the as-fabricated LIG to ensure full coverage. The assembly was pressed using a Carver 4386 hydraulic press at a controlled pressure to allow the encapsulation layer to conform to the graphene structure without excessive structural and electrical degradation. An s-beam load cell was used to monitor the pressure applied. The hydraulic press encapsulation setup is shown in Figure S3, Supporting Information.

 © 2025 The Author(s). Advanced Engineering Materials published by Wiley-VCH GmbH

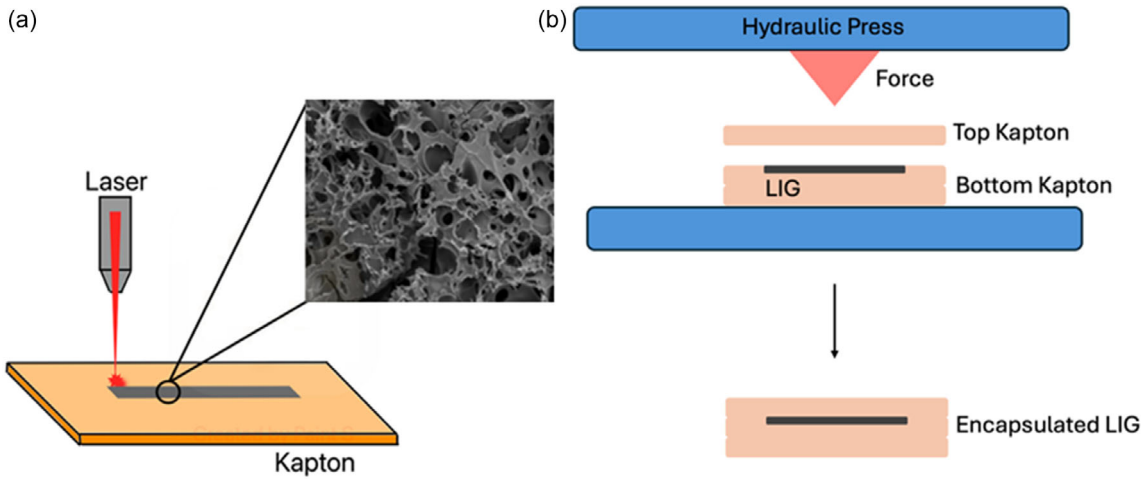

Figure 1. a) Schematic representation of the laser scribing process and the resulting LIG microstructure (inset, SEM image width 200 μm). b). Schematic illustration of the hydraulic press encapsulation process for LIG.

2.3. Resistance Measurement

The electrical resistance of LIG samples was measured using two complementary techniques: two-point and four-point methods. Two-point measurements provide a quick and straightforward resistance measurement by placing silver paint electrodes at a fixed distance along the LIG tracks. However, this method is susceptible to error due to contact resistance introduced at the interface between the silver paint contacts and the graphene surface. To ensure a reliable measurement, four-point measurements were carried out using silver paint contacts arranged in a straight line with equal spacing along the LIG tracks, in order to evaluate the influence of contact resistance. Comparison to two-point measurements is provided in Figure S4, Supporting Information. Comparative measurements were also carried out with an Ossila four-point probe system with similar results. The four-point measurements confirmed that contact resistance was not sizeable enough to alter the trends, and this allowed us to more easily examine the effect of mechanical pressure on the LIG electrical resistance while applying pressure during the encapsulation procedure. The in situ resistance measurement was performed in the hydraulic press to continuously monitor resistance variations. The setup is shown in Figure S3, Supporting Information.

2.4. Raman Spectroscopy Analysis

To characterize the structural integrity of LIG before and after encapsulation, Raman spectroscopy was performed using a Bruker Senterra dispersive Raman microscope equipped with a 532 nm excitation laser. Raman spectroscopy is widely used for graphene-based materials as it provides insights into the degree of graphitization, disorder, and defects within the carbon structure. The analysis focused on key Raman peaks, including the *D* band (≈1350 cm^{-1}), which is associated with structural defects; the *G* band (≈1580 cm^{-1}), which corresponds to in-plane vibrations of sp^2-hybridized carbon atoms; and the 2D band (≈2700 cm^{-1}), which provides information on the number of graphene layers and stacking order.[54–59]

Raman spectra were collected for unencapsulated LIG, as well as for LIG that was compressed using a glass slide under two different pressures: 80 and 780 psi. This allowed us to compress the LIG structure under similar conditions to the encapsulation process while maintaining optical access for Raman microscopy. The intensity ratio of the *D* to *G* bands $I(D)/I(G)$ was used to assess the presence of defects in the structure, while the position and relative intensity of the 2D band were examined to assess the layer characteristics of LIG.[59–63]

2.5. SEM Analysis

Previous studies have shown that unencapsulated LIG typically exhibits a highly porous, 3D interconnected network, a structural feature that contributes to its high surface area and electrical conductivity but also affects its mechanical robustness.[49,64,65] The morphology of laser-induced graphene is known to be influenced by laser processing parameters, with variations in power and scan speed leading to differences in pore size, sheet connectivity, and defect density.[50]

To investigate the morphological features of LIG and the effects of encapsulation, SEM imaging was conducted using a FEI Magellan 400. Imaging was performed at an accelerating voltage of 5 kV with a working distance of 5 mm to obtain high-resolution surface images. SEM imaging was performed on unencapsulated LIG and compressed samples that were subjected to pressures of 80 and 780 psi to evaluate the microstructure under similar conditions to the encapsulation process while maintaining access to the surface for imaging.

2.6. Mechanical Bending Tests

To further investigate the mechanical durability of LIG under repeated deformation, systematic bending cycle tests were conducted. The bending tests aimed to simulate conditions where LIG-based devices would undergo flexing, testing their potential suitability for flexible electronics applications. The samples were subjected to cyclic bending around cylinders having different

© 2025 The Author(s). Advanced Engineering Materials published by Wiley-VCH GmbH

15272648, 0, Downloaded from https://advanced.onlinelibrary.wiley.com/doi/10.1002/adem.202501686, Wiley Online Library on [24/09/2025]. See the Terms and Conditions (https://onlinelibrary.wiley.com/terms-and-conditions) on Wiley Online Library for rules of use; OA articles are governed by the applicable Creative Commons License

curvatures (diameters of 25, 35, and 45 mm). Each sample was tested for 3 bending cycles, and electrical resistance was recorded before bending and after each cycle to monitor potential degradation. While the bending tests in this study focus on 3 cycles as an initial benchmark, future work will include extended-cycle tests to evaluate long-term mechanical performance.

2.7. Environmental Durability Tests

The stability of LIG is a critical factor for its practical implementation in applications, particularly in applications where exposure to environmental factors such as moisture and temperature fluctuations is unavoidable. To evaluate the effectiveness of the encapsulation method in protecting LIG from environmental degradation, durability tests were conducted under controlled humidity conditions. These tests assessed the electrical performance of both encapsulated and unencapsulated LIG samples when directly submerged in water. For these tests, each encapsulated and unencapsulated LIG sample was individually immersed in deionized water for 24 h, as shown in Figure S7, Supporting Information. After immersion, the samples were removed, and their electrical resistance was measured immediately to evaluate potential changes due to water exposure.

3. Results and Discussion

3.1. Electrical Performance of As-Fabricated LIG

The electrical performance of LIG was assessed to determine its baseline conductivity before encapsulation. After optimizing the laser power and scan rate, the average sheet resistance measured was $2.20 \pm 0.14\,\Omega\,\mathrm{sq}^{-1}$ across 24 LIG samples, with individual values ranging from 2.00 to $2.44\,\Omega\,\mathrm{sq}^{-1}$. Notably, the sheet resistance achieved in this study is among the lowest ever reported for LIG, only surpassed by the value obtained by our group using a different laser system and 3D printed polymer substrate[66] and a recent study achieving $1.02\,\Omega\,\mathrm{sq}^{-1}$ using a 3D-printed polymer substrate and a different laser system.[65] Increasing the laser power beyond this threshold resulted in excessive ablation and degradation of the graphene network, whereas lower scan rates led to increased carbonization and loss of conductivity. The optimization of sheet resistance as a function of laser power and scan rate are provided in Figure S1 and S2, Supporting Information. A comparison of the electrical properties of the fabricated LIG with previously reported values is presented in **Table 1**, demonstrating that the proposed fabrication method significantly improves sheet resistance compared to many conventional laser-scribed graphene structures. This is a useful starting point for encapsulation studies, as it represents a low-resistance value that is practically useful to maintain post-encapsulation.

3.2. Effect of Applied Pressure on Resistance

To evaluate the influence of mechanical pressure on the electrical resistance of LIG, samples with silver paint contacts were placed under a glass cover to ensure uniform pressure distribution. In situ resistance measurements were recorded to monitor variations in conductivity as a function of applied pressure. As shown in **Figure 2**a, the resistance of LIG under a single loading/unloading cycle exhibited a nonlinear increase with increasing pressure. At lower pressures (≈80 psi), the resistance changes remained relatively moderate, with a minimum increase of 18%, indicating minimal disruption to the conductive pathways. As pressure increased, a steady upward trend in resistance was observed. The highest applied pressure of 3800 psi resulted in the most significant resistance increase of 195%, suggesting a progressive compression of the LIG network and potential changes in the structure. This result serves as a comparative starting point for the results obtained later in the encapsulation experiment.

Table 1. LIG sheet resistance values obtained in this work compared to previous studies.

Sheet resistance [$\Omega\,\mathrm{sq}^{-1}$]	Reference	Engraving method
2.20 ± 0.14	This work	CO_2 laser on Kapton
7.86	[27]	CO_2 laser on Kapton
10–50	[78]	CO_2 laser on Kapton
120	[79]	CO_2 laser on Kapton
130	[45]	CO_2 laser on polyimide
6.14	[23]	CO_2 laser on PI film
25	[77]	CO_2 laser on PI film
0.3	[66]	CO_2 laser on 3D-printed PEI
15.9	[80]	CO_2 laser on 3D-printed PEI
32	[36]	CO_2 laser on lignin-rich paper
44	[81]	Visible light laser on various substrates
1.02	[65]	Blue laser on pure and 3D-printed PEI and PEEK

To assess the behavior of LIG under repeated mechanical stress, cyclic loading and unloading tests were conducted to evaluate its electrical resistance behavior over multiple pressure cycles. As shown in Figure 2b–d, the resistance exhibited a distinct response pattern across several loading cycles. The first loading cycle caused a significant and irreversible increase in resistance, indicating structural changes within the LIG network. Notably, most of this resistance change occurred during the unloading phase. Subsequent cycles demonstrated a different but more reproducible behavior, applying pressure reduced resistance from the previously established baseline, and upon unloading, the resistance returned to a value that was often slightly higher than before, suggesting minor progressive structural alterations. This trend remained consistent across all pressure levels, with variations in magnitude depending on the applied force.

These findings indicate that LIG undergoes an initial restructuring under mechanical stress and suggests that for applications involving cyclic mechanical stress, an initial conditioning phase may be necessary to stabilize the electrical properties of LIG. After this phase, the material demonstrates predictable and stable behavior, making it suitable for long-term use in flexible or pressure-sensitive devices. However, applications requiring precise resistance stability should account for both the initial irreversible change and the minor progressive shifts over extended cycling.

© 2025 The Author(s). Advanced Engineering Materials published by Wiley-VCH GmbH

15272648, 0, Downloaded from https://advanced.onlinelibrary.wiley.com/doi/10.1002/adem.202501686, Wiley Online Library on [24/09/2025]. See the Terms and Conditions (https://onlinelibrary.wiley.com/terms-and-conditions) on Wiley Online Library for rules of use; OA articles are governed by the applicable Creative Commons License

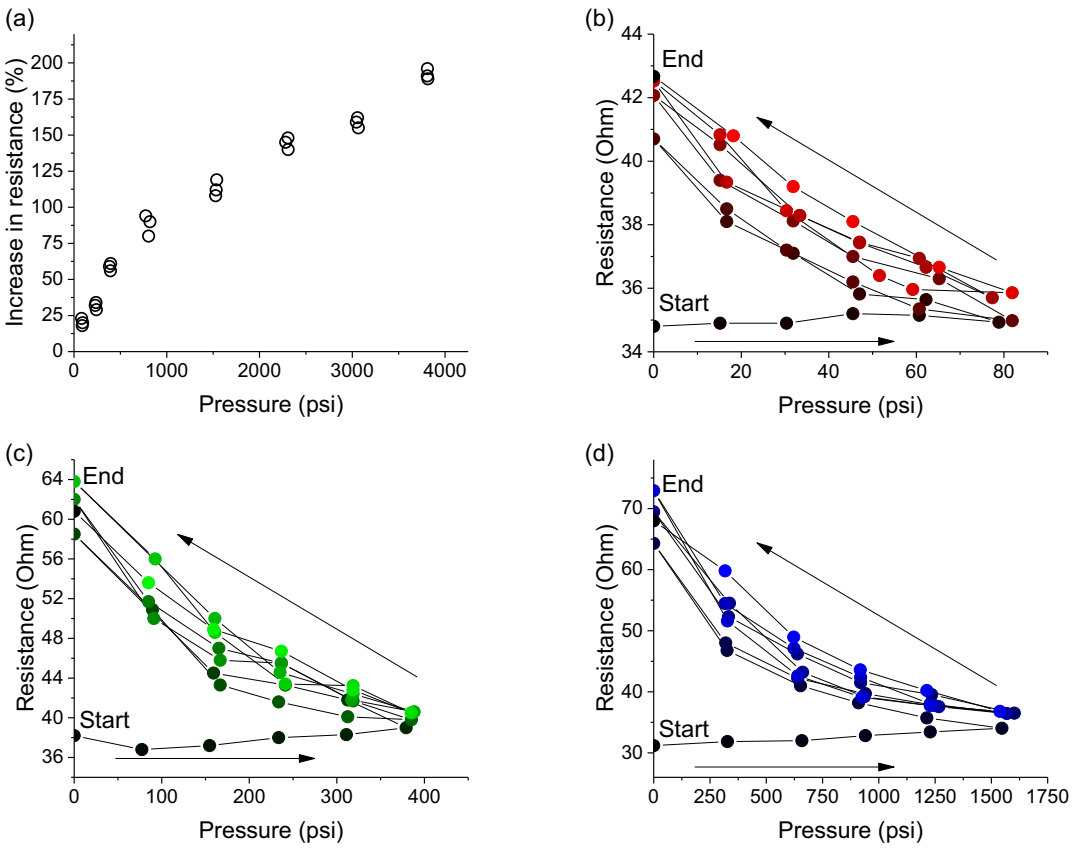

Figure 2. a) Increase in LIG resistance under different static pressures using a glass slide cover. Each data point represents a separate sample exposed to a given static pressure only once. b–d) Cyclic loading/unloading tests showing resistance variations as function of applied pressure for different ultimate pressure conditions: b) 80 psi, c) 400 psi, and d) 1600 psi.

3.3. Effect of Encapsulation on Resistance

To evaluate the impact of encapsulation on LIG's electrical properties during mechanical loading, the resistance was again measured in situ, but this time the encapsulating Kapton layer was used instead of a rigid glass slide. **Figure 3** presents the percent resistance change for encapsulated LIG across a pressure range of 0–4000 psi, showing a significantly lower increase (5–30%) compared to the 20–200% observed in non-encapsulated samples. At pressures below 1000 psi, encapsulated LIG exhibited a minimal resistance increase (5–10%), while at pressures up to 2500 psi, the increase remained within 10–20%. The highest

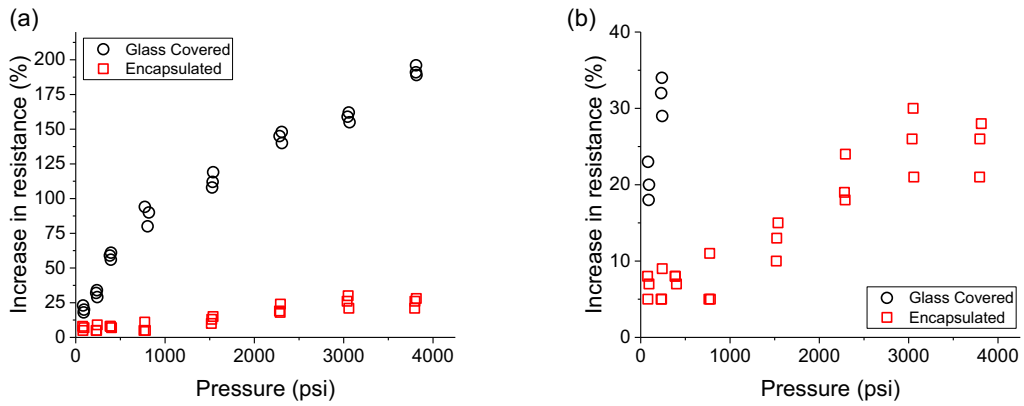

Figure 3. a) Increase in LIG resistance under different static pressures using a glass slide cover (black circles) or encapsulating polyimide (red squares). Each data point represents a separate sample exposed to a given static pressure only once. b) Expanded view of panel (a) to highlight the smaller increase in resistance during encapsulation.

© 2025 The Author(s). Advanced Engineering Materials published by Wiley-VCH GmbH

15272648, 0, Downloaded from https://advanced.onlinelibrary.wiley.com/doi/10.1002/adem.202501686, Wiley Online Library on [24/09/2025]. See the Terms and Conditions (https://onlinelibrary.wiley.com/terms-and-conditions) on Wiley Online Library for rules of use; OA articles are governed by the applicable Creative Commons License

pressure range (3000–4000 psi) resulted in increases between 20 and 30%, demonstrating improved mechanical resilience compared to nonencapsulated samples. The smallest observed resistance change was only 5% at 80 psi, indicating that at this lower pressure, the encapsulation effectively preserves LIG's electrical stability with minimal impact on conductivity.

The encapsulation effectively limits pressure-induced resistance changes by distributing the mechanical stress, preventing localized deformation in the LIG structure. Unlike pressure-loaded nonencapsulated samples, which were only covered by a glass layer and exhibited rapid resistance increases, encapsulated LIG maintained more stable conductivity across a wide pressure range. We propose that the protective effect of Kapton encapsulation arises from its elasticity, which helps distribute pressure more evenly, reducing localized stress points that could compromise LIG's structure.

This study is the first to successfully encapsulate low-resistance LIG ($2.20 \pm 0.14\,\Omega\,\mathrm{sq}^{-1}$) while maintaining minimal resistance increases postencapsulation. These findings underscore the potential of encapsulated LIG for flexible electronics and pressure-sensitive applications, where stable electrical performance under mechanical stress is essential.

3.4. Mechanical and Environmental Stability Tests

To determine the optimal encapsulation condition, the pressure resulting in the least increase in electrical resistance was first identified, indicating that lower pressures are preferable to maintain low resistance. However, it was necessary to determine whether the lowest pressure provided sufficient mechanical integrity and prevent mechanical or environmental degradation. To investigate this, a bending test was conducted on LIG samples encapsulated at different pressures (80–3800 psi) using cylinders of varying diameters (25, 35, and 45 mm) to systematically evaluate the performance under varying pressures with respect to both electrical stability and mechanical robustness.

Each sample was bent over a single cylinder and the resistance was measured before bending, after release, and repeated for three cycles to determine the percent increase in resistance. The data resulting from these tests are tabulated in Table S2, Supporting Information.

As shown in **Figure 4**, increasing the encapsulation pressure led to a greater percentage increase in resistance after three bending cycles, ranging from 64% at 80 psi to 123% at 3798 psi. Larger bending diameters resulted in smaller resistance changes, indicating less mechanical damage due to lower strain. The trend suggests that lower encapsulation pressures (80–400 psi) provide a better compromise between flexibility and electrical stability, with resistance increases remaining around 64–75% after three bending cycles. Higher pressures caused significant increases in resistance both during encapsulation and after bending, making them less suitable for applications requiring mechanical flexibility. We note that most of the irreversible increase in resistance takes place during the first bend and release cycle, with minimal increase afterward, suggesting a similar origin in the relation between structural deformation and resistance increase as observed in the pressure-dependent data in Figure 2.

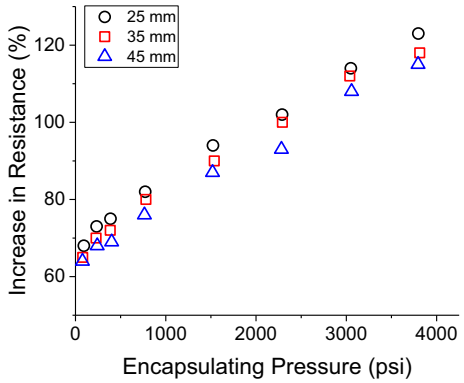

Figure 4. Increase in resistance of encapsulated LIG after bending around cylinders of different diameters: 25 mm (black circles), 35 mm (red squares), or 45 mm (blue triangles). For comparison, the average resistance increases of nonencapsulated LIG for the same bending diameters are 518%, 461%, and 343%, respectively.

For comparison, nonencapsulated LIG was subjected to the same bending test, and the resistance increases were substantially higher, 518% at 25 mm, 461% at 35 mm, and 343% at 45 mm, demonstrating the material's fragility under mechanical stress. Encapsulated samples, in contrast, showed only a 64–123% resistance increase, reinforcing the protective role of encapsulation.

To evaluate the moisture resistance of encapsulated LIG, 10 samples encapsulated at 80 psi were fully immersed in deionized water for 24 h. Initial resistance values were recorded before immersion, and measurements were taken immediately after removal to assess any changes in electrical conductivity. The results, summarized in Table S3 and S4, Supporting Information, show that encapsulated LIG exhibited minimal resistance increases after moisture exposure, with an average increase of $1.0 \pm 0.5\%$ across ten samples. These values indicate strong durability against moisture, suggesting that encapsulation effectively mitigates conductivity degradation in humid environments. For comparison, nonencapsulated LIG underwent the same test and showed a higher average resistance increase of $2.00 \pm 1.15\%$ across 5 samples, as shown in **Figure 5**. To quantify the statistical significance of the effect of encapsulation, a two-sample *t*-test was conducted to compare

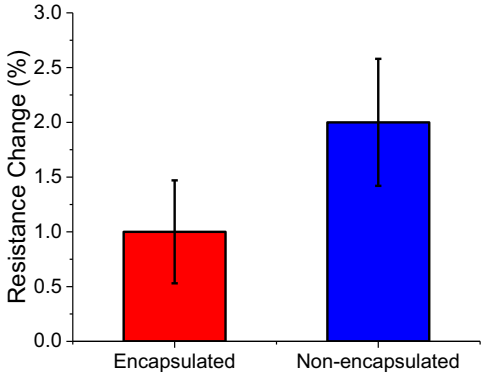

Figure 5. Increase in resistance of LIG after 24 h immersion in deionized water.

© 2025 The Author(s). Advanced Engineering Materials published by Wiley-VCH GmbH

15272648, 0, Downloaded from https://advanced.onlinelibrary.wiley.com/doi/10.1002/adem.202501686, Wiley Online Library on [24/09/2025]. See the Terms and Conditions (https://onlinelibrary.wiley.com/terms-and-conditions) on Wiley Online Library for rules of use; OA articles are governed by the applicable Creative Commons License

resistance changes between encapsulated ($n = 10$) and nonencapsulated ($n = 5$) samples. These results confirm that the encapsulation process enhances LIG's resistance to moisture-induced degradation, making it suitable for applications in environments with high humidity or direct water exposure.

3.5. Raman Spectroscopy Analysis

Raman spectroscopy was used to assess the structural changes in LIG under different encapsulation pressures, providing insights into defect formation, layer stacking, and strain effects. As shown in **Figure 6**, the Raman spectra exhibited three prominent peaks: the *D* peak (≈1350 cm^{-1}), the *G* peak (≈1600 cm^{-1}), and the 2D peak (≈2700 cm^{-1}). The unencapsulated LIG exhibited characteristics of few-layer graphene, with an $I(D)/I(G)$ ratio of 0.862 indicating moderate defect density and an $I(2D)/I(G)$ ratio of 0.721 suggesting multilayer graphene. The full width at half maximum (FWHM) of the 2D peak (69.4 cm^{-1}) further confirmed the few-layer nature, consistent with previous literature.[67–70]

Compression at 80 psi resulted in an increased $I(D)/I(G)$ ratio of 1.286, indicating additional defects, while the $I(2D)/I(G)$ ratio remained relatively stable at 0.789, suggesting minimal impact on graphene stacking. At 780 psi, however, the $I(D)/I(G)$ ratio further increased to 1.323, accompanied by a sharp drop in $I(2D)/I(G)$ to 0.314 and FWHM broadening to 122.4 cm^{-1}. These changes indicate a transition to a more disordered structure with stronger layer coupling and increased strain. **Table 2** summarizes the key Raman parameters for all investigated samples, clearly showing the progressive structural changes with increasing encapsulation pressure.

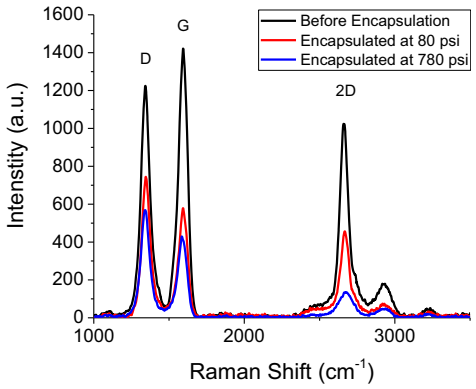

Figure 6. Raman spectra of LIG samples: as prepared (black), after applying 80 psi of pressure (red) and 780 psi of pressure (blue).

Table 2. Summary of Raman spectroscopy parameters for LIG samples under different encapsulation pressures.

Sample	*D* peak position [cm^{-1}]	*G* peak position [cm^{-1}]	2D peak position [cm^{-1}]	$I(D)/I(G)$	$I(2D)/I(G)$	2D FWHM [cm^{-1}]
Before encapsulation	1343.2	1592.7	2663.6	0.862	0.721	69.4
80 psi encapsulation	1346.8	1593.1	2670.1	1.286	0.789	79.3
780 psi encapsulation	1341.9	1588.2	2673.7	1.313	0.314	122.4

The progressive shifts in Raman parameters give clues to the type of structural evolution taking place in LIG under different pressures during the encapsulation process. Low-pressure encapsulation largely preserves the graphene-like character, while high-pressure encapsulation introduces significant defects and disorder. These findings align with previous studies, where increased pressure led to compressive strain effects in grapheme.[71–75] The stability of FWHM values for the *D* and *G* peaks across all samples suggests that the fundamental graphitic structure is maintained, though variations in peak intensity and 2D band broadening indicate changes in interlayer interactions and defect density.[64,76]

These results emphasize that lower encapsulation pressures are preferable for maintaining desirable graphene properties, while excessive pressure compromises structural integrity, which is consistent with electrical resistance results. This analysis provides a foundation for optimizing encapsulation conditions to balance electrical and mechanical performance in LIG-based applications.

3.6. SEM Analysis

SEM imaging was used to analyze the microstructural changes in LIG samples exposed to different pressures. **Figure 7**a shows that unencapsulated LIG exhibits a highly porous, 3D network with interconnected pores. High-magnification images reveal thin, wrinkled graphene sheets forming this structure, which contributes to LIG's high surface area and conductivity. Encapsulation at 80 psi Figure 7b does not alter the microstructure at any magnification level, confirming that low-pressure encapsulation preserves the original structure. This aligns with the minimal resistance change observed post-encapsulation, indicating that the LIG's electrical and morphological properties remain intact.

In contrast, LIG encapsulated at 780 psi Figure 7c exhibits significant structural compression, with a denser network and reduced pore size. Higher magnification images reveal sheet stacking (marked by red circles) and graphene layer fractures (red arrows), indicating increased strain and disorder. This structural transformation aligns with the Raman spectroscopy findings, which show greater defect formation and reduced graphene-like characteristics at higher encapsulation pressures.

These SEM observations confirm that while low-pressure encapsulation maintains the desirable porous structure of LIG, high-pressure encapsulation induces densification, altering its electrical and mechanical properties. The results emphasize the importance of optimizing encapsulation pressure to improve structural integrity and performance.

4. Discussion

Having identified the optimal encapsulation pressure that minimizes resistance increase while maintaining mechanical stability, we can compare the electrical performance of our encapsulated LIG with previously reported encapsulation techniques. Our method resulted in a minimal resistance increase of only 5%, with the initial sheet resistance of about 2.2 Ω sq^{-1}. This is a significant improvement compared to other encapsulation strategies, where

© 2025 The Author(s). Advanced Engineering Materials published by Wiley-VCH GmbH

15272648, 0, Downloaded from https://advanced.onlinelibrary.wiley.com/doi/10.1002/adem.202501686, Wiley Online Library on [24/09/2025]. See the Terms and Conditions (https://onlinelibrary.wiley.com/terms-and-conditions) on Wiley Online Library for rules of use; OA articles are governed by the applicable Creative Commons License

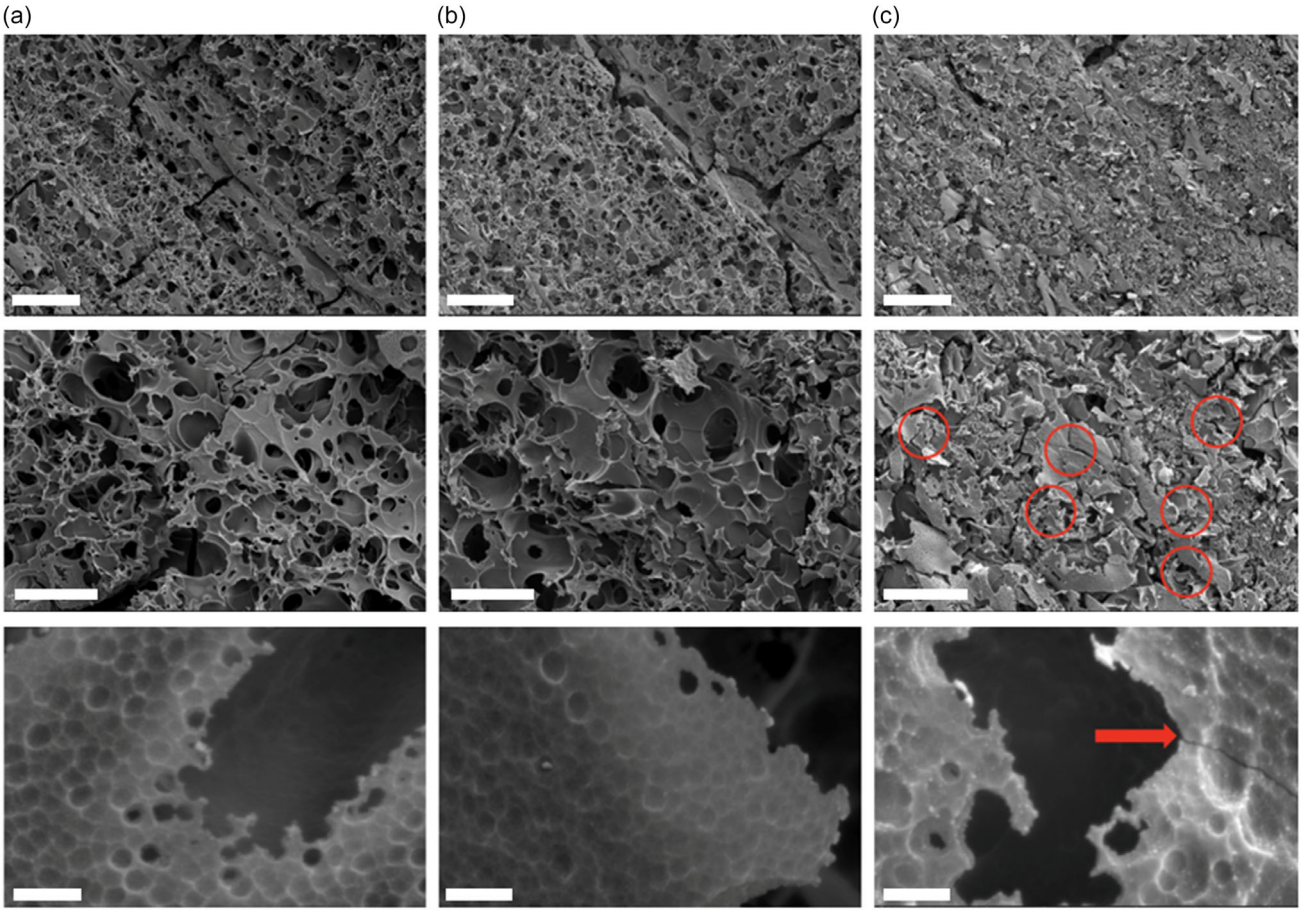

Figure 7. SEM images of LIG samples a) as prepared, b) after applying 80 psi of pressure, and c) after applying 780 psi of pressure. The magnification increases from top to bottom, with scale bars of 100 µm (top), 50 µm (middle), and 1 µm (bottom).

resistance increases range from 154% (duct tape coating) to as high as 1277% (polyurethane coating).[45] LDPE and HDPE coatings resulted in resistance increases of 231% and 269%, respectively, while composite-based approaches, such as LDPE/LIG/HDPE and LDPE/LIG/cheesecloth, led to resistance increases of 262% and 338%, demonstrating the limitations of such encapsulation materials. Given that previous studies did not focus on systematically assessing the resistance changes as a function of encapsulation parameters, we can only speculate on the reasons for the improvements found in this work. The laser scribing conditions being used to prepare the LIG have profound repercussions on the microstructure and electrical properties;[77] therefore, the mechanical deformation of the LIG layer during encapsulation will have varying effects that depend on the initial structure. The increase in resistance we observe as a function of encapsulation pressure points to a disruption of the conduction network in the LIG, and this is a common feature in other encapsulation studies.[45] These studies do not specify the encapsulation pressure used, but based on the methodology utilizing a consumer laminator, this was likely relatively low pressure. Therefore, the smaller increase in resistance after encapsulation we observe here is not likely attributed to smaller applied pressures, although there is a difference in how the pressure is applied (locally using rollers as in ref. 45 or uniformly in our case). We believe the improvement in resistance stems mainly from the initial LIG microstructure, which appears to be more laterally interconnected in our work than the vertical fibers found in ref. 45, and therefore less susceptible to electrical transport disruption over the length of the device. The exceptionally low resistance increase observed with our encapsulation method highlights its superiority in preserving LIG's electrical properties while still providing mechanical reinforcement. These findings indicate that our approach achieves a more effective balance between conductivity retention and encapsulation durability, making it a promising candidate for applications requiring both mechanical stability and high electrical performance.

5. Conclusion

This study has introduced a novel hydraulic press encapsulation technique that significantly enhances the mechanical durability of LIG while maintaining excellent electrical conductivity. The encapsulation process was optimized, resulting in an encapsulated LIG with an initial sheet resistance as low as $2.20 \pm 0.14\,\Omega\,\mathrm{sq}^{-1}$, a minimal increase of only 5% compared to unencapsulated LIG. Our results demonstrate that the encapsulated LIG not only maintains its high conductivity essential for flexible electronics but also shows a remarkable improvement in mechanical robustness.

© 2025 The Author(s). Advanced Engineering Materials published by Wiley-VCH GmbH

15272648, 0, Downloaded from https://advanced.onlinelibrary.wiley.com/doi/10.1002/adem.202501686, Wiley Online Library on [24/09/2025]. See the Terms and Conditions (https://onlinelibrary.wiley.com/terms-and-conditions) on Wiley Online Library for rules of use; OA articles are governed by the applicable Creative Commons License

Cyclic loading tests confirmed that the encapsulated LIG could sustain repeated mechanical stress, retaining its conductive properties effectively. Moreover, the encapsulated LIG exhibited superior resilience to moisture with negligible degradation in performance, showing only a 1% average increase in resistance after 24-h water immersion tests, compared to a 2% increase in unencapsulated samples. Bending tests further showcased the enhanced mechanical stability of the encapsulated LIG, with resistance increases remaining around 75% after the first bending cycle around a 25 mm diameter cylinder. In contrast, the unencapsulated LIG experienced a resistance increase above 500% under similar conditions. Further studies could explore whether these observations persist long-term. The encapsulation technique detailed in this study outperforms existing methods by maintaining over 95% of the electrical performance of LIG while significantly enhancing its mechanical and environmental stability. This method provides a practical, cost-effective, and scalable solution for integrating LIG into various applications, including wearable devices, flexible sensors, and stretchable interconnects, where durability and conductivity are paramount.

Supporting Information

Supporting Information is available from the Wiley Online Library or from the author.

Acknowledgements

The authors acknowledge funding from the Natural Sciences and Engineering Research Council of Canada.

Conflict of Interest

The authors declare no conflict of interest.

Data Availability Statement

The data that support the findings of this study are available from the corresponding author upon reasonable request.

Keywords

electrical conductivity, encapsulation, flexible electronics, laser-induced graphene

Received: June 24, 2025
Revised: September 1, 2025
Published online:

[1] A. Anwar, B. S. Mohammed, M. A. Wahab, M. Liew, *Dev. Built Environ.* **2020**, *1*, 100002.
[2] C. N. R. Rao, K. Biswas, K. Subrahmanyam, A. Govindaraj, *J. Mater. Chem.* **2009**, *19*, 2457.
[3] A. K. Geim, K. S. Novoselov, *Nat. Mater.* **2007**, *6*, 183.
[4] D. R. Cooper, B. D'Anjou, N. Ghattamaneni, B. Harack, M. Hilke, A. Horth, N. Majlis, M. Massicotte, L. Vandsburger, E. Whiteway, V. Yu, *Int. Scholarly Res. Notices* **2012**, *2012*, 501686.
[5] K. S. Novoselov, A. Geim, S. V. Morozov, D. Jiang, Y. Zhang, S. V. Dubonos, I. V. Grigorieva, A. A. Firsov, *Science* **2004**, *306*, 666.
[6] R. Ye, D. K. James, J. M. Tour, *Adv. Mater.* **2019**, *31*, 1803621.
[7] Y. Xu, K. Sheng, C. Li, G. Shi, *ACS Nano* **2010**, *4*, 4324.
[8] M. D. Stoller, S. Park, Y. Zhu, J. An, R. S. Ruoff, *Nano Lett.* **2008**, *8*, 3498.
[9] A. S. Mayorov, R. V. Gorbachev, S. V. Morozov, L. Britnell, R. Jalil, L. A. Ponomarenko, P. Blake, K. S. Novoselov, K. Watanabe, T. Taniguchi, A. K. Geim, *Nano Lett.* **2011**, *11*, 2396.
[10] A. A. Balandin, *Nat. Mater.* **2011**, *10*, 569.
[11] A. A. Balandin, S. Ghosh, W. Bao, I. Calizo, D. Teweldebrhan, F. Miao, C. N. Lau, *Nano Lett.* **2008**, *8*, 902.
[12] A. K. Geim, *Science* **2009**, *324*, 1530.
[13] I. B. Olenych, O. I. Aksimentyeva, L. S. Monastyrskii, Y. Y. Horbenko, M. V. Partyka, A. P. Luchechko, L. I. Yarytska, *Nanoscale Res. Lett.* **2016**, *11*, 1.
[14] Z. Sun, S. Fang, Y. H. Hu, *Chem. Rev.* **2020**, *120*, 10336.
[15] L. Zhang, G. Shi, *J. Phys. Chem. C* **2011**, *115*, 17206.
[16] W. Chen, L. Yan, *Nanoscale* **2011**, *3*, 3132.
[17] K. Sheng, Y. Xu, L. Chun, G. Shi, *New Carbon Mater.* **2011**, *26*, 9.
[18] S. Kumar, N. McEvoy, H. Y. Kim, K. Lee, N. Peltekis, E. Rezvani, H. Nolan, A. Weidlich, R. Daly, G. S. Duesberg, *Phys. Status Solidi B* **2011**, *248*, 2604.
[19] X. Wang, H. You, F. Liu, M. Li, L. Wan, S. Li, Q. Li, Y. Xu, R. Tian, Z. Yu, D. Xiang, J. Cheng, *Chem. Vap. Deposition* **2009**, *15*, 53.
[20] K. Sohn, Y. J. Na, H. Chang, K. M. Roh, H. D. Jang, J. Huang, *Chem. Commun.* **2012**, *48*, 5968.
[21] B. G. Choi, M. Yang, W. H. Hong, J. W. Choi, Y. S. Huh, *ACS Nano* **2012**, *6*, 4020.
[22] Y. Guo, C. Zhang, Y. Chen, Z. Nie, *Nanomaterials* **2022**, *12*, 2336.
[23] J. Lin, Z. Peng, Y. Liu, F. Ruiz-Zepeda, R. Ye, E. L. Samuel, M. J. Yacaman, B. I. Yakobson, J. M. Tour, *Nat. Commun.* **2014**, *5*, 5714.
[24] Z. Dong, Q. He, D. Shen, Z. Gong, D. Zhang, W. Zhang, T. Ono, Y. Jiang, *Microsyst. Nanoeng.* **2023**, *9*, 31.
[25] T. S. D. Le, H. P. Phan, S. Kwon, S. Park, Y. Jung, J. Min, B. J. Chun, H. Yoon, S. H. Ko, S. W. Kim, Y. J. Kim, *Adv. Funct. Mater.* **2022**, *32*, 2205158.
[26] M. G. Stanford, K. Yang, Y. Chyan, C. Kittrell, J. M. Tour, *ACS Nano* **2019**, *13*, 3474.
[27] M. Nazeri, M. Ghalamboran, G. Grau, *Adv. Mater. Technol.* **2023**, *8*, 2300188.
[28] Y. Chyan, R. Ye, Y. Li, S. P. Singh, C. J. Arnusch, J. M. Tour, *ACS Nano* **2018**, *12*, 2176.
[29] R. Ye, Y. Chyan, J. Zhang, Y. Li, X. Han, C. Kittrell, J. M. Tour, *Adv. Mater.* **2017**, *29*, 1702211.
[30] R. Ye, D. K. James, J. M. Tour, *Acc. Chem. Res.* **2018**, *51*, 1609.
[31] Z. Peng, J. Lin, R. Ye, E. L. Samuel, J. M. Tour, *ACS Appl. Mater. Interfaces* **2015**, *7*, 3414.
[32] W. Ma, J. Zhu, Z. Wang, W. Song, G. Cao, *Mater. Today Energy* **2020**, *18*, 100569.
[33] H. Wang, Z. Zhao, P. Liu, X. Guo, *Biosensors* **2022**, *12*, 55.
[34] Z. Wan, N. T. Nguyen, Y. Gao, Q. Li, *Sustainable Mater. Technol.* **2020**, *25*, e00205.
[35] M. G. Stanford, J. T. Li, Y. Chyan, Z. Wang, W. Wang, J. M. Tour, *ACS Nano* **2019**, *13*, 7166.
[36] B. Kulyk, B. F. Silva, A. F. Carvalho, S. Silvestre, A. J. Fernandes, R. Martins, E. Fortunato, F. M. Costa, *ACS Appl. Mater. Interfaces* **2021**, *13*, 10210.
[37] F. M. Vivaldi, A. Dallinger, A. Bonini, N. Poma, L. Sembranti, D. Biagini, P. Salvo, F. Greco, F. Di Francesco, *ACS Appl. Mater. Interfaces* **2021**, *13*, 30245.
[38] S. M. Sharaf, *Advancesn Functionalnd Protective Textiles* (Eds: S. ul-Islam, B. S. Butola), Woodhead Publishing, Duxford, United Kingdom **2020**, *2020*.

© 2025 The Author(s). Advanced Engineering Materials published by Wiley-VCH GmbH

15272648, 0, Downloaded from https://advanced.onlinelibrary.wiley.com/doi/10.1002/adem.202501686, Wiley Online Library on [24/09/2025]. See the Terms and Conditions (https://onlinelibrary.wiley.com/terms-and-conditions) on Wiley Online Library for rules of use; OA articles are governed by the applicable Creative Commons License

[39] S. Zhang, N. Ukrainczyk, A. Zaoui, E. Koenders, *Constr. Build. Mater.* **2024**, *411*, 134536.
[40] F. Tehrani, M. Beltrán-Gastélum, K. Sheth, A. Karajic, L. Yin, R. Kumar, F. Soto, J. Kim, J. Wang, S. Barton, M. Mueller, J. Wang, *Adv. Mater. Technol.* **2019**, *4*, 1900162.
[41] L. Cao, S. Zhu, B. Pan, X. Dai, W. Zhao, Y. Liu, W. Xie, Y. Kuang, X. Liu, *Carbon* **2020**, *163*, 85.
[42] K. Sinha, *Master of Science Thesis*, University of Alberta **2020**.
[43] D. X. Luong, K. Yang, J. Yoon, S. P. Singh, T. Wang, C. J. Arnusch, J. M. Tour, *ACS Nano* **2019**, *13*, 2579.
[44] M. Usman, A. T. Jafry, A. Abbas, G. Hussain, N. Abbas, *Thin Solid Films* **2023**, *780*, 139979.
[45] J. T. Li, M. G. Stanford, W. Chen, S. E. Presutti, J. M. Tour, *ACS Nano* **2020**, *14*, 7911.
[46] C. Melios, C. E. Giusca, V. Panchal, O. Kazakova, *2D Mater.* **2018**, *5*, 022001.
[47] S. F. Shaikh, M. M. Hussain, *Appl. Phys. Lett.* **2020**, *117*, 074101.
[48] S. B. Kalkan, A. Yanilmaz, C. Çelebi, *J. Vac. Sci. Technol., A* **2019**, *37*, 051502.
[49] T. Vićentić, M. Rašljić Rafajilović, S. D. Ilić, B. Koteska, A. Madevska Bogdanova, I. A. Pašti, F. Lehocki, M. Spasenović, *Sensors* **2022**, *22*, 6326.
[50] V. Vojnović, M. Spasenović, I. Pešić, T. Vićentić, M. Rašljić Rafajilović, S. D. Ilić, M. V. Pergal, *Chemosensors* **2025**, *13*, 122.
[51] R. K. Biswas, P. McGlynn, G. M. O'Connor, P. Scully, *Mater. Lett.* **2023**, *343*, 134362.
[52] S. Jeong, Y. Kwon, C. Park, Y. Ito, J. Park, M. S. Hwang, J. Chung, N. Sugita, *Nano Energy* **2024**, *126*, 109663.
[53] A. Lamberti, F. Perrucci, M. Caprioli, M. Serrapede, M. Fontana, S. Bianco, S. Ferrero, E. Tresso, *Nanotechnology* **2017**, *28*, 174002.
[54] A. A. King, B. R. Davies, N. Noorbehesht, P. Newman, T. L. Church, A. T. Harris, J. M. Razal, A. I. Minett, *Sci. Rep.* **2016**, *6*, 19491.
[55] A. C. Ferrari, D. M. Basko, *Nat. Nanotechnol.* **2013**, *8*, 235.
[56] R. Beams, L. G. Cançado, L. Novotny, *J. Phys.: Condens. Matter* **2015**, *27*, 083002.
[57] M. Dresselhaus, A. Jorio, A. Souza Filho, R. Saito, *Philos. Trans. R. Soc., A* **2010**, *368*, 5355.
[58] S. Zhang, J. Wang, Z. Li, R. Zhao, L. Tong, Z. Liu, J. Zhang, Z. Liu, *J. Phys. Chem. C* **2016**, *120*, 10605.
[59] Z. H. Ni, T. Yu, Y. H. Lu, Y. Y. Wang, Y. P. Feng, Z. X. Shen, *ACS Nano* **2008**, *2*, 2301.
[60] J. B. Wu, M. L. Lin, X. Cong, H. N. Liu, P. H. Tan, *Chem. Soc. Rev.* **2018**, *47*, 1822.
[61] Y. Wang, M. Yao, Y. Chen, J. Dong, X. Yang, M. Du, R. Liu, H. Liu, Y. Li, B. Liu, *Appl. Phys. Lett.* **2018**, *113*, 021901.
[62] S. Kim, S. Park, H. Kim, G. Jang, D. Park, J. Y. Park, S. Lee, Y. Ahn, *Appl. Phys. Lett.* **2016**, *108*, 203111.
[63] F. M. Koehler, A. Jacobsen, T. Ihn, K. Ensslin, W. J. Stark, *Nanoscale* **2012**, *4*, 3781.
[64] X. Li, R. U. R. Sagar, L. Zhong, Y. Liu, D. Hui, M. Zhang, *Mater. Lett.* **2019**, *248*, 43.
[65] J. Vandervelde, Y. Yoon, R. Shahriar, S. B. Cronin, Y. Chen, *Small Sci.* **2025**, *5*, 2500022.
[66] M. Tavakkoli Gilavan, M. S. Rahman, A. Minhas-Khan, S. Nambi, G. Grau, *ACS Appl. Electron. Mater.* **2021**, *3*, 3867.
[67] X. W. Xueshen, L. Jinjin, Z. Qing, Z. Yuan, Z. Mengke, *J. Nanomater.* **2013**, *2013*, 101765.
[68] C. Wei, R. Negishi, Y. Ogawa, M. Akabori, Y. Taniyasu, Y. Kobayashi, *Jpn. J. Appl. Phys.* **2019**, *58*, SIIB04.
[69] N. Gupta, S. Walia, U. Mogera, G. U. Kulkarni, *J. Phys. Chem. Lett.* **2020**, *11*, 2797.
[70] Y. Stubrov, A. Nikolenko, V. Strelchuk, S. Nedilko, V. Chornii, *Nanoscale Res. Lett.* **2017**, *12*, 1.
[71] L. X. Duy, Z. Peng, Y. Li, J. Zhang, Y. Ji, J. M. Tour, *Carbon* **2018**, *126*, 472.
[72] Z. Sun, A. R. O. Raji, Y. Zhu, C. Xiang, Z. Yan, C. Kittrell, E. Samuel, J. M. Tour, *ACS Nano* **2012**, *6*, 9790.
[73] D. A. Sokolov, K. R. Shepperd, T. M. Orlando, *J. Phys. Chem. Lett.* **2010**, *1*, 2633.
[74] N. Ferralis, R. Maboudian, C. Carraro, *Phys. Rev. Lett.* **2008**, *101*, 156801.
[75] N. Sharma, D. Oh, H. Abernathy, M. Liu, P. N. First, T. M. Orlando, *Surf. Sci.* **2010**, *604*, 84.
[76] J. de la Roche, I. López-Cifuentes, A. Jaramillo-Botero, *Carbon Lett.* **2023**, *33*, 587.
[77] A. Minhas-Khan, S. Nambi, G. Grau, *Carbon* **2021**, *181*, 310.
[78] H. Le, A. Minhas-Khan, S. Nambi, G. Grau, W. Shen, D. Wu, *Flexible Printed Electron.* **2023**, *8*, 035013.
[79] J. L. Beckham, J. T. Li, M. G. Stanford, W. Chen, E. A. McHugh, P. A. Advincula, K. M. Wyss, Y. Chyan, W. L. Boldman, W. D. Rack, J. M. Tour, *ACS Nano* **2021**, *15*, 8976.
[80] L. Jiao, Z. Y. Chua, S. K. Moon, J. Song, G. Bi, H. Zheng, J. Koo, *Nanomaterials* **2019**, *9*, 90.
[81] Z. Zhang, M. Song, J. Hao, K. Wu, C. Li, C. Hu, *Carbon* **2018**, *127*, 287.

© 2025 The Author(s). Advanced Engineering Materials published by Wiley-VCH GmbH

15272648, 0, Downloaded from https://advanced.onlinelibrary.wiley.com/doi/10.1002/adem.202501686, Wiley Online Library on [24/09/2025]. See the Terms and Conditions (https://onlinelibrary.wiley.com/terms-and-conditions) on Wiley Online Library for rules of use; OA articles are governed by the applicable Creative Commons License